Cargo encapsulated hepatitis E virus-like particles for anti-HEV antibody detection

Cargo encapsulated Hepatitis E virus-like particles for anti-HEV antibody detection

Akhilesh Babu Ganganboina[1], Kenshin Takemura[2], Wenjing Zhang[3], Tian-Cheng Li[3], Enoch Y. Park[1,2,*]

[1] Research Institute of Green Science and Technology, Shizuoka University, 836 Ohya Suruga-ku, Shizuoka 422-8529, Japan

[2] Department of Bioscience, Graduate School of Science and Technology, Shizuoka University, 836 Ohya Suruga-ku, Shizuoka 422-8529, Japan

[3] Department of Virology 2, National Institute of Infectious Diseases, 4-7-1 Gakuen, Musashimurayam-shi, Tokyo 208-0011, Japan

E-mail addresses:
akhilesh.babu.ganganboina@shizuoka.ac.jp (ABG)
takemura.kenshin.16@shizuoka.ac.jp (KT)
zwjviolin@foxmail.com (WZ)
litc@nih.go.jp (TCL)
park.enoch@shizuoka.ac.jp (EYP)

[*] Corresponding author at: Research Institute of Green Science and Technology, Shizuoka University, 836 Ohya, Suruga-ku, Shizuoka 422-8529, Japan.
E-mail address: park.enoch@shizuoka.ac.jp (E.Y. Park). Tel (Fax): +81-54-238-4887)

Abstract

Viral capsid-nanoparticle hybrid structures incorporating quantum dots (QDs) into virus-like particles (VLPs) constitute an emerging bioinspired type of nanoarchitecture paradigm used for various applications. In the present study, we packed inorganic QDs in vitro into the hepatitis E virus-like particle (HEV-LP) and developed a fluorometric biosensor for HEV antibody detection. Firstly, for the preparation of QDs-encapsulated HEV-LPs (QDs@HEV-LP), the HEV-LPs produced by a recombinant baculovirus expression system were disassembled and reassembled in the presence of QDs using the self-assembly approach. Thus, the prepared QDs@HEV-LP exhibited excellent fluorescence properties similar to QDs. Further, in the presence of HEV antibodies in the serum samples, when mixed with QDs@HEV-LP, bind together and further bind to anti-IgG-conjugated magnetic nanoparticles (MNPs). The target-specific anti-IgG-MNPs and QDs@HEV-LP enrich the HEV antibodies by magnetic separation, and the separated QDs@HEV-LP-bound HEV antibodies are quantified by fluorescence measurement. This developed method was applied to detect the HEV antibody from sera of HEV-infected monkey from 0 to 68 days-post-infection and successfully diagnosed for HEV antibodies. The viral RNA copies number from monkey fecal samples by RT-qPCR was compared to the HEV antibody generation. This study first used QDs-encapsulated VLPs as useful fluorescence emitters for biosensing platform construction. It provides an efficient route for highly sensitive and specific antibody detection in clinical diagnosis research.

Keywords: Virus-like particles, quantum dots, antibody, fluorescence, infectious disease diagnosis, hepatitis E virus.

1. Introduction

Nanoparticles and biomaterial conjugates exhibit several highly beneficial properties that can be used for biosensing (Michalet et al., 2005; Tagit et al., 2017; Yang et al., 2020). Viral capsids have drawn considerable interest in the field of nanobiology due to their symmetrical structure, nanoscale size, and controllable self-assembly with easy modifications (Herbert et al., 2020; Sasaki et al., 2020). The virus-based nanoparticles, integrating the bio-activities of virus capsids with nanoparticle functions, are a recently emerging class of bio-nanomaterials with many potential applications, such as theranostics, bio-imaging, biosensing, and advanced synthesis of nanomaterial (Brasch et al., 2017; Li et al., 2019a; Liu et al., 2012; Yan et al., 2015). One application is the continuous monitoring of viral infection, which might prevent the spread of viral infection. Inspired by nature, virus-based nanoparticles encapsulated with various materials like inorganic nanoparticles, proteins, nucleic acids, and small molecule drugs are developed to fabricate new kind of nanostructures (Chen et al., 2005; Dixit et al., 2006; Li et al., 2019a; Li et al., 2011).

The primary technique for encapsulation is the reassembly of virus-like particles (VLPs) in the presence of materials of interest. Initially, VLPs are dissociated into subunit oligomers (building blocks) by treating with suitable buffers, followed by mixing the oligomers with cargoes and buffer exchange to accelerate the VLPs reassembly encapsulating the cargo (Aniagyei et al., 2009; Brasch et al., 2017). Dragnea et al., (2003). demonstrated a similar self-assembly technique encapsulating gold nanoparticles in the Brome mosaic virus's capsids. VLPs obtained from bacteriophage MS2, Qbeta, and hepatitis B virus (HBV) are highly stable and have received significant attention in nanotechnology (Liu et al., 2012; Wen and Steinmetz 2016). Recent developments in preparing multifunctional nanomaterials pave the way for integrating various detection methodologies (Chowdhury et al., 2018; Dang et al., 2020; Dutta Chowdhury et al., 2018; Ganganboina and Doong 2019). The encapsulation of nanomaterials

in VLPs from different viruses can improve biocompatibility, making VLPs attractive nanocapsule for various nanomaterials' encapsulation (Ma et al., 2012). QDs-encapsulated VLPs exhibit strong luminescence allowing them to be used as promising luminescent bioprobes. However, the insufficient focus has been paid on applying virus-based nanoparticles loaded with various cargoes concerning prepared virus-based nanoparticles' stability.

Antibodies are well known as essential biomarkers for many disorders, including infectious diseases, autoimmune diseases, and allergies (Arts et al., 2016; Lei et al., 2018). Detection of antibodies in low concentrations with straight forward using highly reliable assays urgently needs appropriate clinical treatment. However, immobilized antigen on solid supports leads to the physical deformation of antigen, hampering the detection sensitivity of several disease-specific antibodies in enzyme-linked immunosorbent assays (ELISAs), lateral flow assays, or protein microarrays (Ganganboina et al., 2020a; Tsai et al., 2016; Zhang et al., 2014). In addition, the uncertain orientation of antigens deposited can mask essential epitopes for antibody conjugation (Iverson et al., 2002). Solution-phase techniques like radioimmunoassay (RIA) is the current gold standard antibody detection method with significant advantages. The highly sensitive RIAs use highly radioactive reagents and demand laborious washing and centrifugation steps. In addition, the poor multiplexing ability of RIAs limits the application for development of new antibody biomarkers (Qi and Zhang 2019). As a result, currently, existing methods do not satisfy the need for an assay that maintains the native conformation of antigens and allows efficient, multiplexed identification of their related antibodies. Such an approach will significantly enhance disease identification diagnostic techniques confirming the sensitive antibody biomarkers and promoting under-explored biomarkers in multiple human pathologies.

Hepatitis E virus (HEV) is a non-enveloped RNA virus that causes self-limiting acute process illness with reported chronic hepatitis cases. HEV causes chronic infections in

immunocompromised people and is transfusion-transmissible (Liu et al., 2020). The World Health Organization identifies the HEV infection as a public health problem in several developing countries, especially among at-risk communities such as pregnant women, displaced persons living in camps, and epidemic situations (Ganganboina et al., 2020c; World Health Organization, 2015). The serological diagnosis of acute HEV infection is based on identifying HEV-specific IgM antibodies or recent reoccurrence or dramatic increase in virus-specific IgG antibody titers. However, commercially available HEV antibody assays show significant disparities in sensitivity and specificity (Wenzel et al., 2013; Zafrullah et al., 2018). This highlights the need for accurate testing to diagnose acute or past HEV infections.

To overcome the limitations of the existing antibody detection methods, a sensing platform using QDs-encapsulated VLPs has been developed. As a new nano-biomaterial class, VLPs are considered possible biological carriers to encapsulate QDs due to their high similarity in conformation and natural virus properties, which aid in biosensing. In this study, HEV-like particles (HEV-LPs) are primarily used as a model to apply the principle of QD encapsulation to HEV-based protein cages. A robust and sensitive assay for the detection of HEV antibodies was developed using the QD-encapsulated HEV-LPs. VLPs contain protein sequences that are related to the binding between virus and cell surface receptors. Thus, VLPs can mimic native virus binding against its specific antibody. In addition, the solution phase detection method developed in this study, maintains the native conformation of antigens. It avoids the unexpected orientation, which can withhold the essential epitopes for antibody conjugation and prevent antigens physical deformation after immobilization on solid supports. The optimized fluorometric biosensing platform achieved high sensitivity for the anti-HEV antibody assay. Significantly, this study not only revealed QDs-encapsulated HEV-LPs (QDs@HEV-LPs) as promising fluorescence emitters for biosensing platform development but also opened a new

avenue for highly sensitive and selective antibody detection in disease diagnosis and clinical research.

2. Materials and methods

2.1 Preparation of CdSeTeS quantum dots and biomaterials

The quaternary alloyed CdSeTeS QDs are synthesized using a one-step organometallic hot-injection technique by modifying the synthesis method discussed in our previous study (Adegoke et al., 2015).

Anti-white spot syndrome virus (WSSV) VP28 antibody [ab26935] were purchased from Abcam Inc. (Cambridge, UK). Anti-influenza virus (IFV) antibody (New Caledonia/20/99) (H1N1) from IFV was purchased from Prospec-Tany Techno Gene Ltd. (Rehovot, Israel). Anti-norovirus (NoV) antibody broadly reactive to genogroup II (NS14 Ab) were provided by Prof. T. Suzuki of Hamamatsu University School of Medicine (Hamamatsu, Japan). Anti-S protein antibody of SARS-CoV-2 were purchased from GeneTex, Inc. CA, USA. Anti-NS1 protein antibody for zika virus (ZIKV) (MAB12312-100) and anti-E1 protein of Chikungunya virus (CHIKV) (NAT41557-100) were purchased from the Native Antigen company (Oxford, United Kingdom).

2.2 Construction of a recombinant baculovirus.

Genotype 1 (G1) HEV strain (GenBank accession no.: DQ079624) was isolated from an acute hepatitis E patient in Myanmar in 1986. PCR-amplified DNA fragments with N-

139 terminal 111 amino acid deletions encoded by ORF2 with two primers, HEV-D13 (5'-
140 AAGGATCCATGGCGGTCGCTCCAGCCCATGACACCCCGCCAGT-3) and HEV-U14
141 (5'-GGTCTAGACTATAACTCCCGAGTTTTACCCACCTTCATCTT-3). The product
142 obtained from PCR included the XbaI site after the stop codon and the BamHI site before the
143 start codon. Purification of the PCR product was performed using a QIAquick Gel Extraction
144 Kit (Qiagen, Hilden, Germany) and cloned into TA cloning vector pCR2.1 (Invitrogen,
145 Carlsbad, CA, USA), digested with BamHI and XbaI, and ligated with a baculovirus transfer
146 vector, pVL1393 (Pharmingen, San Diego, CA, USA), to yield plasmid pVL5480/7126. The
147 transition plasmid pVL5480/7126 to the recombinant baculovirus was combined with
148 baculoGold (Pharmingen) and lipofectin (GIBCO-BRL, Gaithersburg, MD, USA) and
149 transfected into Sf9 insect cells (Riken Cell Bank, Tsukuba, Japan). Cells were incubated in
150 TC-100 medium (GIBCO-BRL) complemented with 10% fetal bovine serum (FBS) at 26.5 °C
151 and 0.26% tryptose phosphate broth (Difco Laboratories, Sparks, MD, USA). Recombinant
152 baculovirus was plaque-purified three times in Sf9 cells and identified as Ac5480/712657 (Li
153 et al., 1997).

154

155 *2.3 Expression and purification of HEV-LPs.*

156 Cells from the *Trichoplusia ni*, BTL-Tn 5B1–4 (Tn5) cell line, were infected with the
157 Ac5480/7126 at a multiplicity of infection 10 and grown at 26.5 °C in EX-CELL 405 medium
158 (JRH Biosciences, Lenexa, KS, USA). Later, the Tn5 cells were harvested at 7 days-post-
159 infection (dpi). By centrifugation for 60 min at 10,000 × g, the intact cells and cell debris were
160 removed. The supernatant was then separated by spinning in a Beckman SW32Ti rotor at
161 100,000 × g for 3 h, and the resulting pellet was resuspended at 4 °C overnight in EX-CELL
162 405 medium. Further, 4.5 mL of each sample was combined with 2.1 g of CsCl and centrifuged

with a Beckman SW55Ti rotor at 100,000 g for 24 h at 10 °C. The gradient was divided into 250-μL aliquots and weighted each fraction to approximate the buoyant density and isopycnic value. To separate the CsCl, each fraction was diluted with an EX-CELL 405 medium and centrifuged in a Beckman TLA55 rotor for 2 h at 100,000 g (Yang et al., 2017).

2.4 Rabbit anti-G3 HEV IgG antibody generation.

Japanese white rabbits were immunized with 500 μg of G3 HEV-LPs by percutaneous injection. In addition, booster injections were given at 4 and 6 weeks after the first injection with half doses of G3 HEV-LPs. All of the injections, including booster injections, were administered without using adjuvant. Blood was collected from immunized animals 3 weeks after the last injection, and the anti-HEV-LPs IgG was purified by protein G column (Li et al., 2011).

2.5 Preparation of QDs-encapsulated HEV-LPs.

The QDs are encapsulated into HEV-LPs according to a procedure described previously with slight modifications (Takamura et al., 2004). A 180 μl of a buffer containing 50 mM Tris-HCl (pH 7.5), 150 mM NaCl, 1 mM EGTA, and 20 mM dithiothreitol was used to disrupt the purified VLPs (50 μg). After 30 min of incubation at room temperature, various concentrations of QDs in 50 mM Tris-HCl buffer (pH 7.5) and 150 mM NaCl were added to the above mixture. The disturbed VLP preparation was regenerated by incubation for 1 h, with increased $CaCl_2$ concentrations up to 5 mM. VLPs were purified by ultracentrifugation and resuspended in 10 mM potassium-MES buffer (pH 6.2). After negative staining, the development of QDs@HEV-LPs structures was confirmed by electron microscopy at each step.

The unencapsulated QDs were removed by dialysis. Various mixtures were transferred into a 10 kDa dialysis bag, placed in a buffer (40 mM Tris-HCl, 150 mM NaCl, 1 mM $CaCl_2$, pH 7.4), and stirred overnight at 4 °C. The dialysis bag solution was then collected and centrifuged at 20000 × g, 4 °C for 1 h, to spin down the QDs@HEV-LPs.

2.6 Sodium dodecyl sulfate-polyacrylamide gel electrophoresis (SDS-PAGE) and Western blotting.

The protein of HEV-LPs was separated by SDS-PAGE using 5–20% e-Page (ATTO, Tokyo) and then stained with Coomassie blue. For western blotting, the separated protein was electrophoretically transferred onto a nitrocellulose membrane. The membrane was blocked with 5% skim milk in 50 mM Tris-HCl (pH 7.4) containing 150 mM NaCl, and then incubated with 1: 2,000 diluted rabbit anti-HEV-LPs antibody. Detection of the rabbit IgG antibody was achieved using alkaline phosphatase-conjugated affinity-purified goat anti-rabbit IgG (H+L) (1:1000 dilution) (Chemicon, USA). Nitroblue tetrazolium chloride and 5-Bromo-4-chloro-3-indolyl phosphate P-toluidine were used as coloring agents (Bio-Rad Laboratories, Hercules, CA).

2.7 Preparation of amine-functionalized magnetic nanoparticles (MNPs).

Amine-functionalized MNPs (Amine-MNPs) were synthesized according to the method described by Robinson and Stevenson (2013) with some modifications. A solution of $NH_2C_6H_{12}NH_2$ (2.2 g), KAc (0.78 g), and $FeCl_3 \cdot 6H_2O$ (0.33 g) in ethylene glycol (10 mL) was transferred into a Teflon-lined autoclave and reacted at 180 °C for 5 h. The precipitated amine-MNPs were then rinsed with ethanol and water (3 times each).

209

210 *2.8 Preparation of anti-rabbit IgG antibody-conjugated MNPs and anti-monkey IgG antibody-*
211 *conjugated MNPs*

212 The anti-rabbit-IgG-conjugated amine-MNPs were prepared using EDC/NHS reaction
213 mentioned in our previous work (Ganganboina et al., 2020b). Briefly, the prepared amine-
214 MNPs in PBS were mixed with 0.1 M EDC to activate the carboxylic group to ester-
215 intermediate form and was mixed with excess 0.4 M NHS and 5.1 µg of anti-rabbit (R)-IgG
216 antibody solution. Finally, the mixture was then stirred overnight at 7 °C. The anti-R-IgG
217 antibody-conjugated MNPs (Anti-R-IgG@MNPs) were separated magnetically from the
218 mixture of unreacted chemicals, and were stored at 4 °C for further use. Like the procedure
219 mentioned above, anti-monkey (M)-IgG antibody-conjugated MNPs (Anti-M-IgG@MNPs)
220 were prepared, replacing the anti-R-IgG antibody with anti-M-IgG antibody (Nordic-MUbio,
221 Susteren, Netherlands) and used for detecting the HEV antibodies in samples obtained from
222 cynomolgus monkey.

223

224 *2.9 Inoculation of cynomolgus monkeys and sample collection.*

225 Nonhuman primates, including cynomolgus monkeys, are widely used in animal
226 models to study HEV infection, pathogenesis, and vaccine trials. The sensor performance has
227 been tested G5 HEV-infected cynomolgus monkey (Li et al., 2019b). A 10-year old male
228 cynomolgus monkey, which was negative for HEV RNA by a nested broad-spectrum RT-PCR
229 and negative for anti-HEV antibodies were intravenously inoculated with 1 mL of the G5 HEV
230 through the femoral vein. The serum samples were collected 2 times per week until 5 weeks
231 p.i. and then collected weekly until 10 weeks p.i. and used to detect anti-G5 HEV IgG

antibodies. The fecal samples were collected daily until 35 dpi and then collected weekly and used to detect the G5 HEV RNA using RT-PCR.

2.10 Characterizations.

Transmission electron microscopy (TEM), dynamic light scattering (DLS), X-ray diffraction (XRD) patterns, X-ray photoelectron spectroscopy (XPS), UV/Vis absorption spectra, and fluorescence measurements were performed using the instruments described in our previous studies (Dutta Chowdhury et al., 2018).

2.11 Detection of anti-HEV antibodies.

QD@HEV-LPs were mixed with different concentrations of the anti-HEV Rabbit IgG antibodies obtained from Japanese white rabbits immunized with HEV and further incubated for 20 min. Later, anti-R-IgG-conjugated-MNPs were mixed with the above solution and further incubated for 20 min. Magnetic separation was applied to capture anti-R-IgG@MNPs/anti-HEV antibody/QD@HEV-LPs complex. The anti-IgG@MNPs/anti-HEV antibody/QD@HEV-LPs complex was separated magnetically, followed by washing several times with phosphate-buffered saline (PBS) to remove all unbound QD@HEV-LPs. After the separation, the mixture was re-dispersed into fresh 100 μL PBS buffer, and the fluorescence intensity was measured using a fluorescence spectrometer (Infinite F200 M; TECAN, Ltd, Männedorf, Switzerland). The sample solution was excited at 450 nm, and the fluorescence intensity was measured in a range of 580 – 720 nm. To monitor anti-HEV antibodies in serum samples from HEV-infected cynomolgus monkeys, a similar procedure as mentioned above

was performed, however, replacing anti-M-IgG-conjugated to MNPs (anti-M-IgG@MNPs) instead of anti-R-IgG@MNPs.

2.12 Quantitative real-time RT-PCR for detection of G5 HEV

The RNA extraction was carried out by a MagNA Pure LC System with a MagNA Pure LC Total Nucleic Acid isolation kit (Roche Applied Science, Mannheim, Germany). A TaqMan assay for determination of the G5 HEV RNA copy number was performed using a 7500 FAST Real-Time PCR System (Applied Biosystems, Foster City, CA) with TaqMan Fast Virus 1-step Master Mix (Applied Biosystems) and the forward primer 5'-CCATGGAGGCCCACCAGTT-3'(nt 24–42), a reverse primer 5'-TCAGGGCGAAAGACCAGCTG-3' (nt 185–204), and probe 5'-FAM-CCAACTCCGCCTTGGCGAATGC-TAMRA-3' (nt 96–117). One-step quantitative RT-PCR (RT-qPCR) was performed for 5 min at 50 °C and for 20 s at 95 °C, followed by 50 cycles of 3 s at 95 °C and 30 s at 60 °C. A 10-fold serial dilution of the capped G5 HEV RNA, 10 to 107 copies, was used as the standard. Amplification data were collected and analyzed with Sequence Detector software version 1.3 (Applied Biosystems).

3. Results and discussion

3.1 Working principle

Scheme 1 exhibits the newly developed fluorometric sensing system's basic concept for the reliable and ultrasensitive detection of anti-HEV IgG antibody. It consists of QDs@HEV-LPs and anti-M-IgG@MNPs that can precisely identify anti-HEV antibody and

form the complex structure of QDs@HEV-LPs/Anti-HEV antibody/Anti-M-IgG@MNPs, as shown in **Scheme 1**. Following the interaction, the nanoconjugates of QDs@HEV-LPs/Anti-HEV/Anti-M-IgG@MNPs are separated magnetically from the excess reagents and other interfering substances. In thus formed sandwich-like structure with QDs@HEV-LPs/Anti-HEV antibody/Anti-M-IgG@MNPs, Anti-M-IgG@MNPs isolate the target antibodies, and QDs@HEV-LPs amplify the signal.

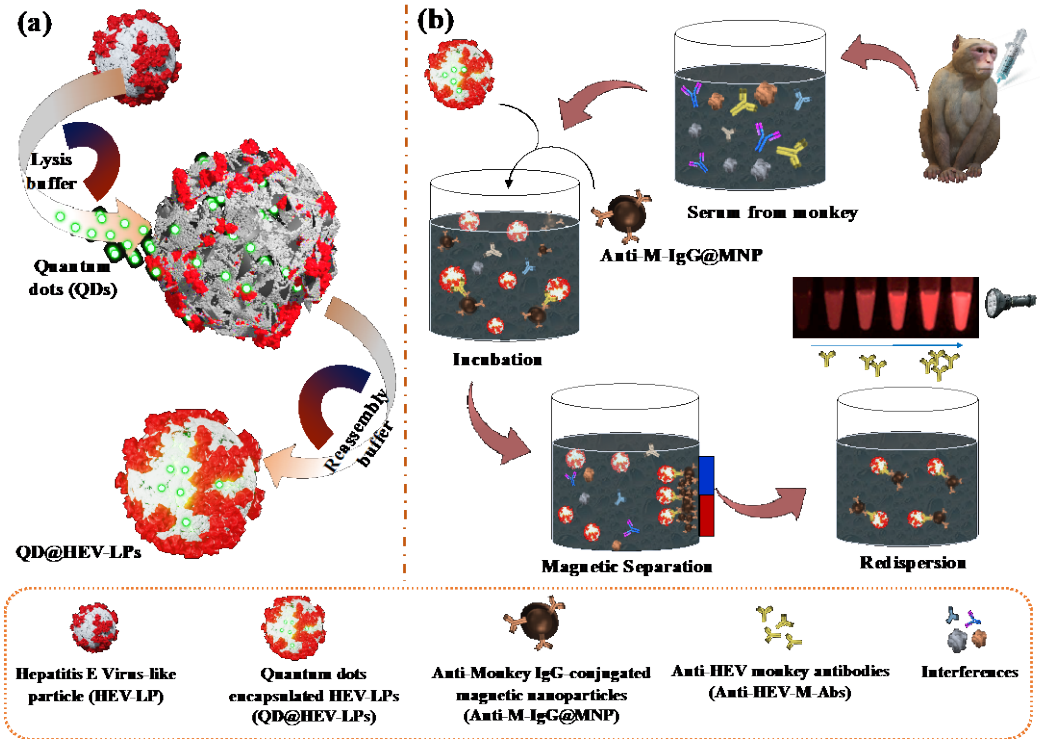

Scheme 1. Schematic representation illustrating the **(a)** fabrication process of QDs-encapsulated the HEV-LPs (QD@HEV-LPs), and **(b)** target anti-HEV antibody detection principle based on antigen-antibody reaction and magnetic separation.

Owing to the existence of QDs within the HEV-LPs, the QDs@HEV-LPs have excellent fluorescence efficiency. This fluorescence is used as a signal to ensure the sensitivity and

accuracy of sensing the target virus. Thus, separated complex dispersed into a fresh buffer is used to record the fluorescence intensity. The increase in the target antibody concentration facilitates an increased number of QDs@HEV-LPs with the target antibody and further with anti-R-IgG@MNPs, increasing fluorescence intensity. The absence of target antibody cannot form the target/QDs@HEV-LPs complex resulting in the negligible presence of QDs@HEV-LPs in the separated mixture causing no change in fluorescence intensity. The developed QDs@HEV-LPs-based sensor will provide superior accuracy, diversity, and flexibility to fulfill the detection needs in diverse regions and diverse circumstances. Encapsulated QDs inside the HEV-LPs are not influenced by the external matrix allowing the identification of sensitive fluorometric signal readings and the target's magnetic separation, benefit the detection capabilities in low analyte concentration and complex matrix.

3.2 Characterizations of QDs, HEV-LPs, and QDs@HEV-LPs

The synthesis of QD@HEV-LPs involves three steps, as illustrated in **Fig. 1a**: i) synthesis of QDs and preparation of HEV-LPs, ii) disassembly of HEV-LPs, and iii) reassembly of HEV-LPs in the presence of QDs. **Fig. 1b** shows the TEM image of CdSeTeS QDs. For the preparation of HEV-LPs, the culture medium of Ac5480/7126-infected Tn5 cells is collected at 7 dpi, and CsCl-gradient centrifugation was performed to purify p53 (Li et al., 1997; Li et al., 2011). The TEM images of HEV-LPs showed uniformly dispersed spherical particles with an average diameter of approximately 35 nm (**Fig. 1c).** The morphology of these particles is similar to that of HEV native particles. The purified HEV-LPs are disassembled by reducing disulfide bonds using DTT (**Fig. 1d**). Further, when calcium ions were introduced to the disassembled HEV-LPs mixture in the presence of QDs, the QDs are encapsulated into the

refolded HEV-LPs (**Fig. 1e**). As observed from the TEM images, no significant morphological difference has occurred due to the HEV-LPs disrupting and refolding process.

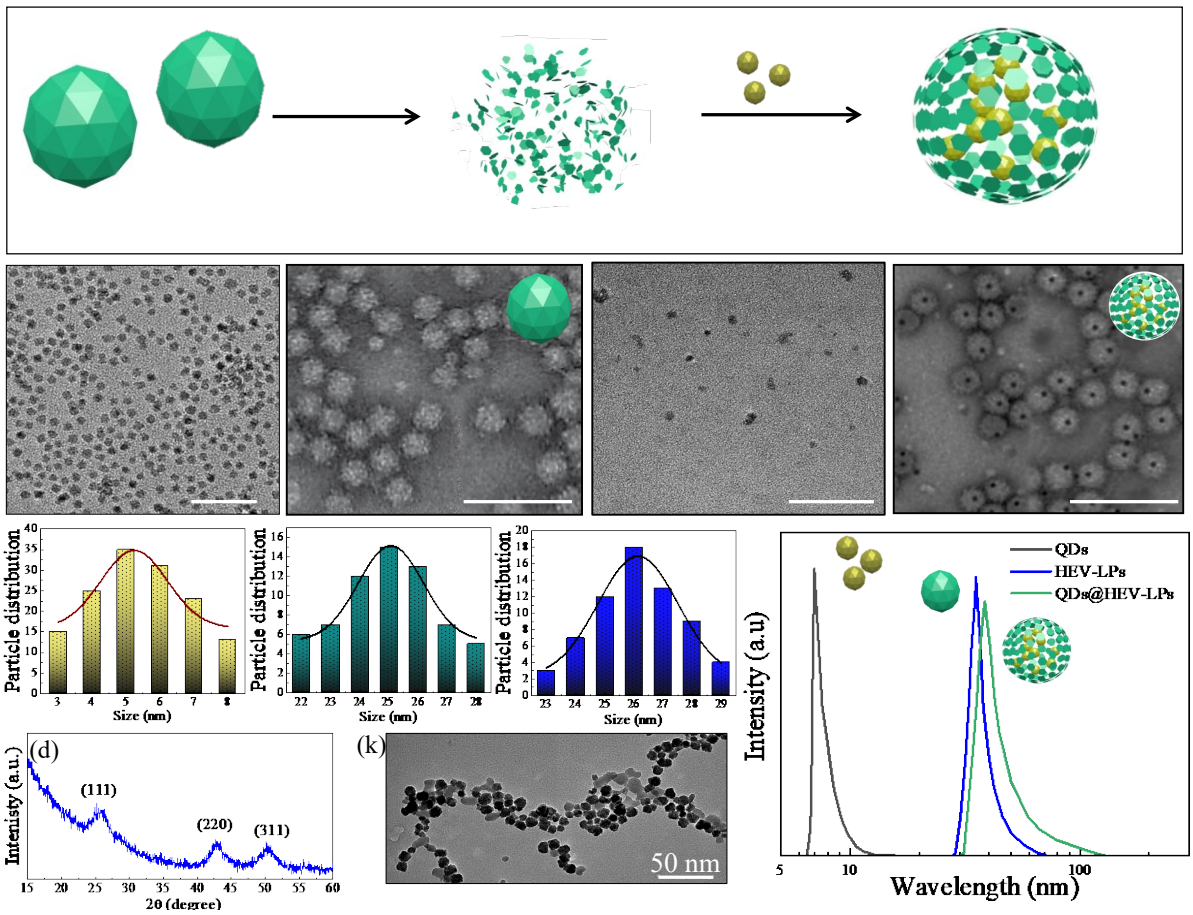

Fig. 1. Synthesis and characterization of QD@HEV-LPs. **(a)** Schematic illustration of the synthesis steps preparing the QD@HEV-LPs. The TEM images of **(b)** QDs, **(c)** HEV-LPs**, (d)** disassembled HEV-LPs, **(e)** QD@HEV-LPs, and corresponding particle size distributions of **(f)** QDs, (**g**) HEV-LPs, and (**h**) QD@HEV-LPs, **(i)** DLS measurement of QDs (black), HEV-LPs (blue), and QD@HEV-LPs (green), **(j)** XRD of QDs and **(k)** TEM image of MNPs.

The synthesized CdSeTeS QDs are circular, with particle size between 3 to 8 nm and an average particle diameter of 5 nm (**Fig. 1f**). The HEV-LPs are morphologically uniform with

small size distribution and a mean diameter of 25 nm (**Fig. 1g**). TEM images clearly show the QD@HEV-LPs are morphologically uniform with a mean diameter of 26 nm and narrow size distribution (**Fig. 1h**). Dynamic light scattering (DLS) analysis also confirmed the size homogeneity of QDs, HEV-LPs, and QD@ HEV-LPs with a mean hydrodynamic diameter of 7.0, 36.0, and 38.0 nm, respectively (**Fig. 1i**). The comparatively small particle size distribution is in agreement with the optical measurements. X-ray diffraction (XRD) is analyzed to measure the crystal nature. The diffraction pattern of the QDs suggests that the QDs are crystalline (**Fig. 1j**), showing three characteristic peaks for (111), (220), and (311) crystal planes at 2theta of 24.7°, 42.4°, and 50.4°, respectively (Adegoke et al., 2015). As shown in **Fig. 1k**, the synthesized amine-functionalized MNPs (Amine-MNPs) are spherical with a diameter range of 15 and 20 nm.

The HEV-LP proteins in the fractions of the CsCl gradient centrifugation were confirmed by western blotting analysis (**Fig. 2a**) and SDS-PAGE (**Fig. 2b**). The binding of the HEV-specific primary antibody used in western blotting corresponded to the full-length HEV-LPs (**Fig. 2a**) and the single band shown in Coomassie Blue staining indicates that the purification is highly efficient (**Fig. 2b-i**). Furthermore, SDS-PAGE confirmed that the same bands as the HEV-LPs mentioned above were obtained in each step of the preparation of QD@HEV-LPs (**Fig. 2b**). **Fig. 2c** displays the fluorescence spectra of pristine QDs and QDs@HEV-LPs. QDs@HEV-LPs show a shift in emission wavelength of around 6–8 nm concerning pristine QDs alone. We assume that the encapsulation of QDs in the viral capsid induces an increase in the effective refraction index (Dixit et al., 2006). The fluorescence intensity of QDs decreased several folds after the preparation of QD@HEV-LPs (**Fig. S1**) as the unencapsulated QDs are separated, and also the protein coat on the surface of the QDs might also interfere with the fluorescence intensity of the QD@HEV-LPs. The stability QDs@HEV-LP solution is evaluated by storing the prepared QDs@HEV-LP at 4 °C for 20

days by monitoring the change in fluorescence intensity periodically. As shown in **Fig. S2**, the fluorescence intensity of QDs@HEV-LP was stable for 10 days and recovery was determined to be 93%. After 15 and 20 days of storage, the QDs@HEV-LP can retain the original fluorescence intensity of 84 and 79%, respectively. In addition, the antibody binding affinity for HEV-LPs and QD@HEV-LPs was confirmed using a conventional ELISA system with IgG-HRP as shown in **Fig. S3**. The binding affinity of QD@HEV-LPs was not decreased before and after assembly.

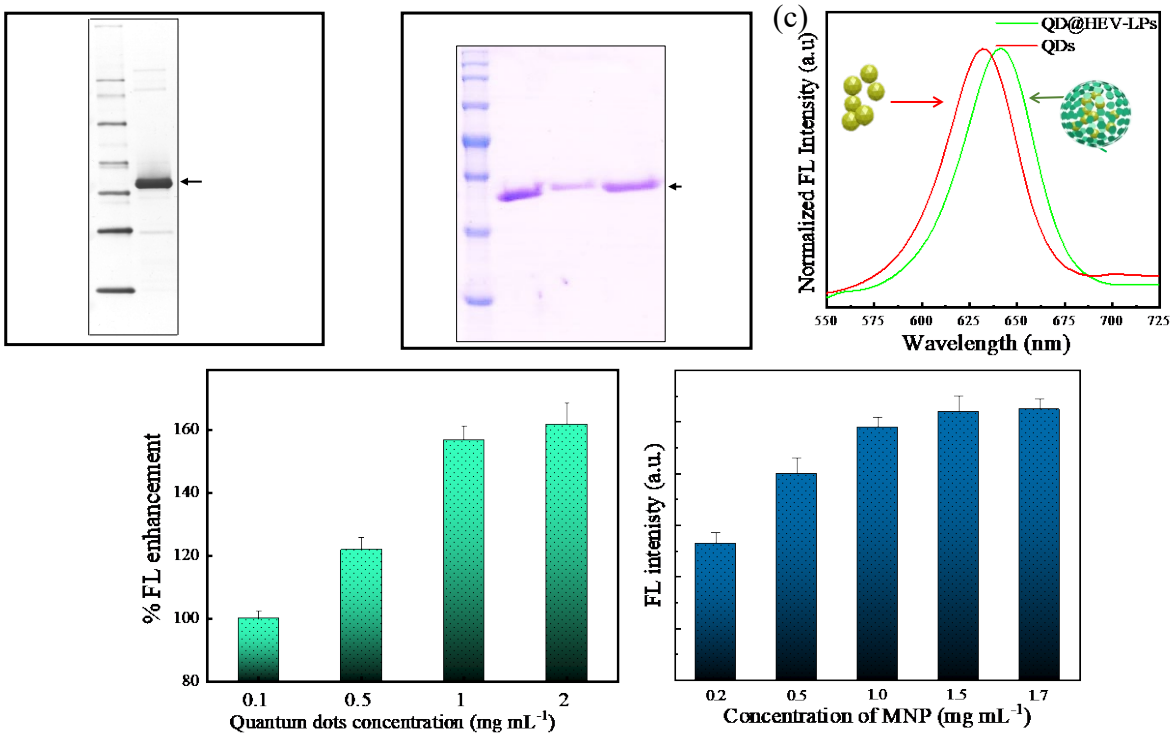

Fig. 2. Western blot of HEV-LPs (**a**) and SDS-PAGE of HEV-LPs (i), disassembled HEV-LPs (ii), and QD@HEV-LPs (iii) (**b**). **(c)** Fluorescent emission spectra of QDs (red) and QDs@HEV-LPs (green). Optimizations of QDs concentration on the fluorescence of prepared QD@HEV-LPs **(d)** and MNP concentration for the QDs@HEV-LP/anti-HEV-Ab/anti-IgG-HEV@MNPs nanoconjugates **(e)** in HEV antibody sensing. Error bars in d and e denote data as average ± SD (n = 3).

366 *3.3 Feasibility of anti-HEV antibody detection using QDs@HEV-LPs.*

367 The amount of QDs used for the preparation of QDs@HEV-LPs is optimized with the
368 fixed amount of HEV-LPs (**Fig. 2d)**. In the case of 0.5 and 1 mg mL^{-1} QDs concentration, the
369 fluorescence intensity is quite satisfactory and almost saturated in higher than 1 mg mL^{-1}. The
370 assembly reaction might contain few incompletely formed capsids and some protein/QD
371 amorphous aggregation, resulting in increased fluorescence intensity. A similar phenomenon
372 has been reported in the formation of VLPs with Au cores; when the cores are presenting excess,
373 incomplete protein coverage occurs (Chen et al., 2005). Therefore, QDs concentration of 1 mg
374 mL^{-1} was chosen to prepare the QDs@HEV-LPs.

375 In addition, the fewer amount of MNPs cannot bind all the antibodies along with
376 QDs@HEV-LPs, leading to false signals. Therefore, optimization of the MNPs concentration
377 is also a crucial parameter in this work. A concentration of 10^{-9} g mL^{-1} of anti-HEV antibody
378 is tested with different amounts of MNPs with a fixed concentration of QDs-HEV-LPs. As
379 shown in **Fig. 2e**, the magnetically isolated QDs@HEV-LPs||anti-HEV antibody||anti-R-
380 IgG@MNPs have been tested by the fluorometric method. In the case of a low amount of anti-
381 R-IgG@MNPs, the magnetic nanoconjugates contain a lesser amount of QDs@HEV-LPs as
382 compared to the 1 mg, which indicates the partial attachment of QDs@HEV-LPs||anti-HEV
383 antibody complex. On the other hand, a high amount of MNPs of 1.5 and 1.7 mg, though the
384 magnetic adduct successfully separated the HEV-LPs. However, itself-quenched the signal due
385 to the QDs@HEV-LPs and MNP interaction. Therefore, optimizing all the results, 1 mg of
386 anti-R-IgG@MNPs shows the best-optimized antibody detection condition.

387

388 *3.4 Sensitivity of anti-HEV antibody detection*

389 The quantitative measurement is performed by detecting various anti-HEV antibodies'
390 concentrations under the optimal conditions to determine the sensitivity of the proposed
391 fluorescence dependent biosensor. It can be seen from **Fig. 3a**; the fluorescence intensity
392 increased proportionally with the increasing anti-HEV antibody concentrations from 10^{-13} g
393 mL^{-1} to 10^{-7} g mL^{-1}. The linear relationship between the fluorescence intensities changes and
394 the logarithmic values of anti-HEV concentration is plotted in **Fig. 3b**, and the detection limit
395 was estimated at 87 fg mL^{-1} calculated using mean of blank sample added to 3.3 times standard
396 deviation of the lowest concentration of target (Armbruster and Pry 2008; Ganganboina and
397 Doong 2018, 2019; Ganganboina et al., 2018). In addition, the calibration curve shows
398 acceptable linearity with a correlation coefficient (R^2) of 0.986. These results strongly
399 demonstrate that the QDs@HEV-LPs-based sensor possesses a strong anti-interference ability,
400 high accuracy, and improved sensitivity.

401 The anti-HEV antibody detection sensitivity of the developed QD@HEV-LPs-based
402 sensor is competitive with recently developed sensing methods (**Table S1** of Supplementary
403 data). In our developed sensor, using QD@HEV-LPs exhibits the following benefits. VLPs
404 containing receptor-binding domain to cell surface receptors can mimic native virus favoring
405 the specific binding between antibody and target virus. Above all, the native conformation of
406 antigens maintains during the detecting procedure in the solution phase. It prevents the
407 unexpected orientation not withholding the necessary epitopes for antibody conjugation and
408 prevents the physical deformation of antigen after immobilization on supports. VLPs resemble
409 native viruses, thereby providing repetitive antigens on the surface of VLPs, providing
410 significant advantages over other antibody detection platforms. Besides being safe and
411 efficacious, VLPs also provide the added advantage of multivalency by combining closely
412 related VLPs in desired concentrations into a single formulation which will further help to
413 develop multiple antibody detection using the same VLPs. In addition, ease as well as

consistency of production using stable cell lines provides easy scale-up and commercialization. This is the first study demonstrating the effectiveness of QDs-encapsulated VLPs antibody detection to the best of our knowledge.

3.5 Effect of a complex matrix on anti-HEV antibody detection using QDs@HEV-LPs

To establish a reliable and practical immunoassay, a dilution series of anti-HEV antibody concentrations are spiked in the biological human serum matrix. The developed fluorometric biosensor shows a linear increase of fluorescence intensity to the function of the introduced anti-HEV antibodies in the medium (**Fig. 3c**). **Fig. 3d** shows the calibration line for anti-HEV antibody detection using the human serum as a detection medium. The gradient of the calibration line is slightly flat shifted than the linear calibration from the anti-HEV antibody detection in buffer solution up to 15%. However, the anti-HEV antibody detection's responsive linearity confirmed the applicability of the developed antibody biosensor in a sophisticated serum matrix. The interfering substances in human serum samples do not react and hamper the fluorescence intensity of QD@HEV-LPs. Prompt to the matrix effect, the calibration curve slope is flattened, increasing the LOD value 1.13 pg mL^{-1}. However, the higher LOD due to the matrix effect is considerable compared to the previously reported results for its real application (Bohm et al., 2020; Shrestha et al., 2016; Takahashi et al., 2005). In addition, to evaluate the sensitivity of the developed method with traditional ELISA, we have performed the ELISA using QD@HEV-LPs and HRP-conjugated anti-rabbit IgG to detect the anti-HEV antibodies. As shown in Fig. S4, the change in absorbance from 1 pg mL^{-1} of anti-HEV antibody can be observed. However, change in absorbance intensity of 0.1 pg mL^{-1} of an anti-HEV is very small or almost negligible, limiting the sensitivity of ELISA using QD@HEV-

LPs to 1 pg mL^{-1}. However, in the developed method, anti-HEV antibody can be detected from 1 fg mL^{-1} to 100 ng mL^{-1}, attributing to the developed method's increased sensitivity.

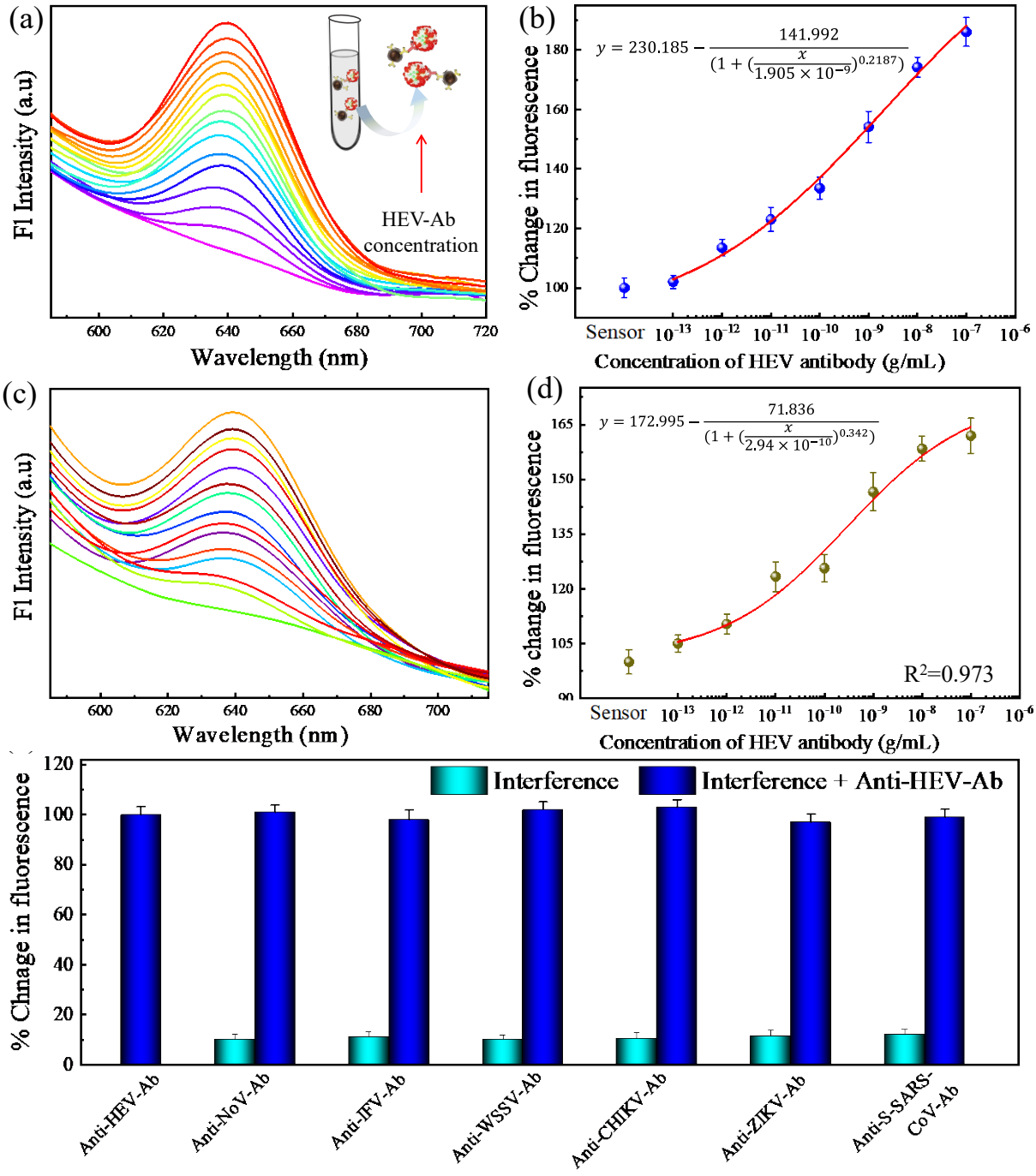

Fig. 3. Sensitivity test of QD@HEV-LPs-based fluorometric sensor for anti-HEV antibody. (**a**) Change in fluorescence spectra of QD@HEV-LPs in the presence of different concentrations of anti-HEV antibodies, (**b**) calibration curve, change of fluorescence intensities of QD@HEV-LPs vs. anti-HEV antibody concentration, (**c**) fluorescence spectra, and (**d**) calibration curve for anti-HEV antibodies in 10% human serum as a sensing medium. (**e**) Selectivity test in the presence of the target anti-HEV antibody and other antibodies. Error bars in b, d and e denote data as average ± SD (n = 3).

3.6 Specificity of anti-HEV antibody detection

The selectivity of the developed QDs@HEV-LPs-based fluorometric biosensor for anti-HEV antibody detection is evaluated. The anti-VP28 antibody for WSSV, anti-IFV antibody (New Caledonia/20/99) (H1N1) for IFV, Anti-S protein antibody of SARS-CoV-2 obtained from rabbit, anti-NoV antibody broadly reactive to genogroup II (NS14 Ab), anti-NS1 protein antibody for ZIKV, and anti-E1 protein of CHIKV antibodies obtained from mouse are assayed as interferences (negative samples) to examine the anti-interference effect and the selectivity of the developed biosensor which is collated to the response of anti-HEV antibody. **Fig. 3e** shows the change in the fluorescence intensity of the developed biosensor to the negative samples and anti-HEV antibody. The analytical signal was developed for the sample containing the only anti-HEV antibody, but not in the negative samples containing interferences only. The interfering antibodies are unrecognizable by the QDs@HEV-LPs, which are specific to the anti-HEV antibody. After magnetic separation and washing, there are no QDs@HEV-LPs in the reaction chamber, resulting in a small increase in the fluorescence intensity. The only slight increase in the analytical signal in detecting the negative samples justified the superior

specificity of QDs@HEV-LPs-based fluorometric sensors towards anti-HEV antibody detection.

3.7 Detection of anti-HEV-IgG from the serum samples and RNA copy number from fecal specimens of G5-HEV-infected cynomolgus monkey

Considering the high sensitivity and accuracy of the developed method for anti-HEV antibody detection, it was further applied to evaluate the applicability in sera of G5-HEV-infected cynomolgus monkey. Sera were collected from 0 to 68 dpi. As shown in **Fig. 4a**, the change in fluorescence intensity started at 7 dpi, indicating that the anti-HEV antibodies were first induced at 7 dpi. Using the calibration curve established (**Fig. 3b**), the concentration of anti-HEV was estimated. At 7 dpi, 1.4 pg mL^{-1} of anti-HEV was found in a serum sample. The change in fluorescence intensity further increased, measuring 54.5 pg mL^{-1} of anti-HEV antibodies on the 19 dpi and then remained constant until 25 dpi. The anti-HEV antibody concentration further increased after 25 dpi and measured to be 110 pg mL^{-1} at 33 dpi, reached a plateau after 40 dpi with anti-HEV antibody concentration of 149 pg mL^{-1}.

In addition, to measure the HEV RNA concentration in G5-HEV-infected cynomolgus monkey, RNA copy numbers of fecal specimens collected from 0 to 68 dpi were measured by RT-qPCR. After the second to third weeks, the infection peak is shown and then gradually decreased to an undetectable amount after the fourth week. As shown in **Fig. 4b**, the G5-HEV was detected 2.66×10^4 copies mL^{-1} in the fecal specimen on 9 dpi, and then it reached a peak of 1.54×10^6 copies mL^{-1} on 20 dpi, and it started to decrease later. The RNA copy number was undetectable after 30 dpi.

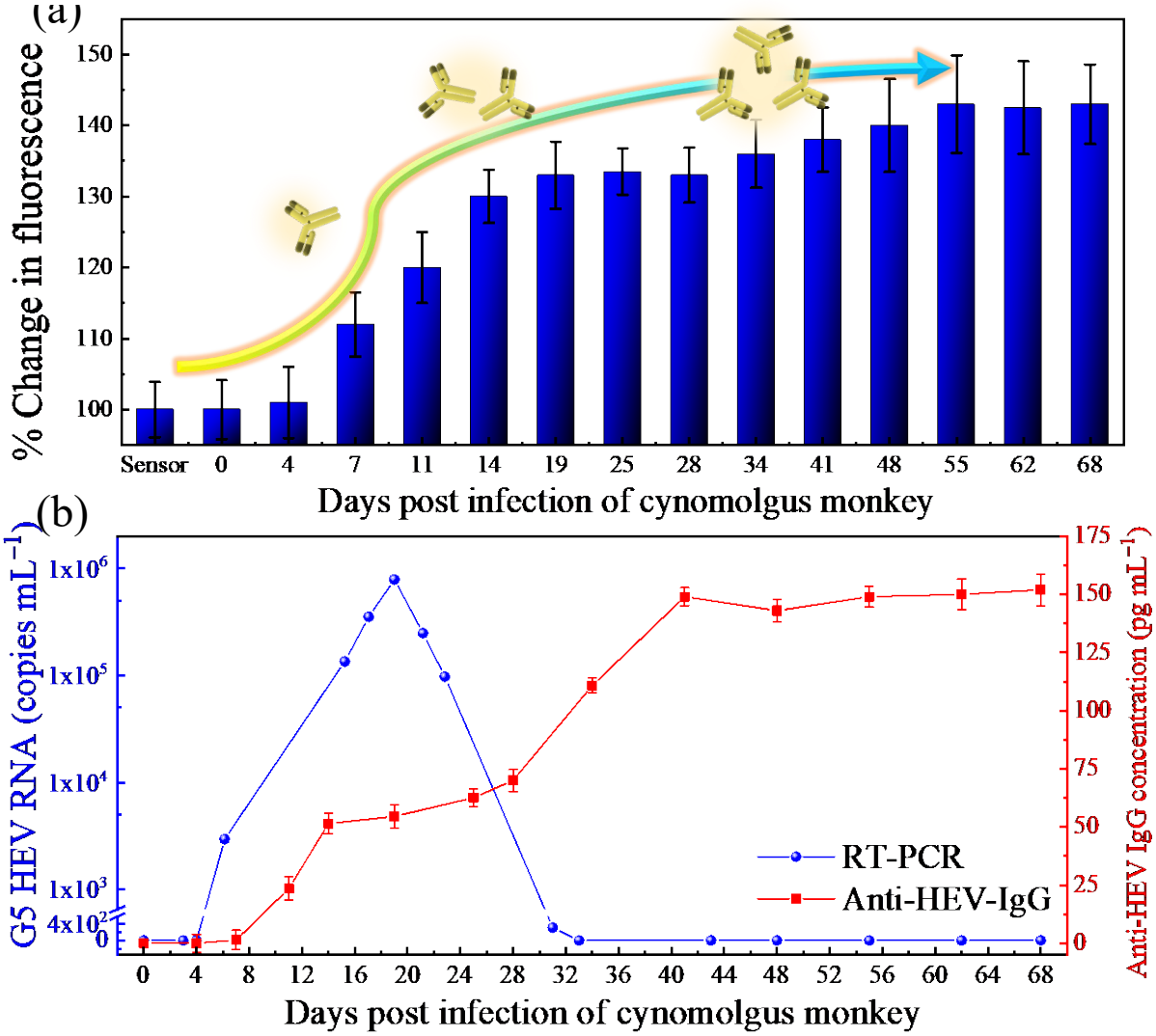

Fig. 4. G5 HEV infection in cynomolgus monkey and sensor performance. (**a**) Change in fluorescence of QD@HEV-LPs in the presence of sera of G5 HEV-infected cynomolgus monkey, (**b**) comparison of the anti-HEV IgG concentration in serum and respective G5-HEV RNA concentration in fecal specimens of G5 HEV-infected cynomolgus monkey. The sera and fecal specimens were collected at 0–68 dpi from an experimentally G5 HEV-infected cynomolgus monkey. Error bars in b, d and e denote data as average ± SD (n = 3).

Comparison of the HEV RNA copy numbers in feces and anti-HEV antibodies concentration in serum from day 0 to 68 dpi, (**Fig. 4b**) clearly shows that the infection could be controlled in the infected monkey immediately after the increase in anti-HEV IgG antibody

497 concentration in sera after 19 dpi. The IgG concertation increased until 40 dpi and remained at
498 high levels until 68 dpi. Resulting, no further change in HEV RNA copy numbers and remained
499 undetected after 30 dpi in the feces samples. The anti-HEV antibody concentration detected in
500 HEV-infected monkey using the developed fluorescence method follow the similar trend with
501 the O.D. values measured using the gold standard ELISA technique (Li et al., 2019b),
502 confirming the applicability of the developed sensing method for real samples. This newly
503 developed strategy builds a useful capability for fluorescence-based convenient screening and
504 accurate diagnosis of suspect infections.

505

506 **4. Conclusions**

507 In conclusion, we have demonstrated an effective method for assembling QD@HEV-
508 LPs, profiting by encapsulating fluorescent QDs into HEV-LPs with high specificity for
509 antibody detection. The unique bio-nanomaterial, QD@HEV-LPs, preserves the fluorescence
510 of the incorporated QDs and also provides uniform dispersibility. The QD@HEV-LPs are
511 successfully applied for the low-level anti-HEV antibody detection, using the universal
512 antigen-antibody conjugation. The specificity for HEV antibodies is obtained from the HEV-
513 LPs, and the encapsulated QDs provide analytical signals. The strong magnetic responsive
514 ability of anti-IgG@MNPs favors the efficient separation of the target from complex samples
515 without any pretreatment. As a result, amplified fluorescence readout from the enriched
516 QDs@HEV-LP/anti-HEV antibody/anti-IgG@MNPs is attained. The developed fluorometric
517 sensor can assay the HEV antibodies with a detection limit down to 87 fg mL^{-1}. The developed
518 sensor showed excellent performance for detecting antibodies in the complex matrix without
519 eliciting observable interference. Moreover, it is successfully applied for the detection of
520 antibodies in sera from HEV-infected monkey. Importantly, this work is the first to investigate

the QDs@HEV-LP's fluorescence behavior for biosensing platform construction and offered an efficient way for highly sensitive and selective detection anti-HEV antibody. The developed method would open up new possibilities for developing nanomaterials-loaded VLPs with suitable functions. It would benefit the advancement of nanotechnologies based on VLPs in disease diagnosis and clinical research.

CRediT authorship contribution statement

ABG designed this study and wrote the paper. ABG and KT fabricated QD@HEV-LPs, characterized, collected, and analyzed experimental data. TCL prepared HEV-LP and provided HEV-infected sera, RT-qPCR. EYP conceived this study, revised paper, and supervised this study. All authors commended on the manuscript.

Ethics declarations

The animal experiments were reviewed and approved by the National Institute of Infectious Diseases (NIID) Ethics Committee and carried out according to the "Guides for Animal Experiments Performed at NIID" under codes 110054 and 514014.

Declaration of competing interest

The authors declare that they have no competing financial interests.

Acknowledgement

NoV antibodies were kindly provided by Professor T. Suzuki of Department of Infectious Diseases, Hamamatsu University School of Medicine. ABG and KT sincerely thanks the Japan Society for the Promotion of Science (JSPS) for a postdoctoral fellowship (Grant Nos. 19F19064 and 20J13223).

References

Adegoke, O., Nyokong, T., Forbes, P.B., 2015. J. Alloys Compd. 645, 443–449.

Aniagyei, S.E., Kennedy, C.J., Stein, B., Willits, D.A., Douglas, T., Young, M.J., De, M., Rotello, V.M., Srisathiyanarayanan, D., Kao, C.C., 2009. Nano Lett. 9(1), 393–398.

Armbruster, D.A., Pry, T., 2008. Clin. Biochem. Rev. 29(Suppl 1), S49.

Arts, R., Den Hartog, I., Zijlema, S.E., Thijssen, V., van der Beelen, S.H., Merkx, M., 2016. Anal. chem. 88(8), 4525–4532.

Bohm, K., Strömpl, J., Krumbholz, A., Zell, R., Krause, G., Sievers, C., 2020. J. Clin. Microbiol. 58(2), e01029-19.

Brasch, M., Putri, R.M., de Ruiter, M.V., Luque, D., Koay, M.S., Castón, J.R., Cornelissen, J.J., 2017. J. Am. Chem. Soc. 139(4), 1512–1519.

Chen, C., Kwak, E.-S., Stein, B., Kao, C.C., Dragnea, B., 2005. J. Nanosci. Nanotechnol. 5(12), 2029–2033.

Chowdhury, A.D., Ganganboina, A.B., Tsai, Y.-c., Chiu, H.-c., Doong, R.-a., 2018. Anal. Chim. Acta 1027, 109–120.

Dang, V.D., Ganganboina, A.B., Doong, R.-A., 2020. ACS Appl. Mater. Interfaces 12(29), 32247–32258.

Dixit, S.K., Goicochea, N.L., Daniel, M.-C., Murali, A., Bronstein, L., De, M., Stein, B., Rotello, V.M., Kao, C.C., Dragnea, B., 2006. Nano Lett. 6(9), 1993–1999.

566 Dragnea, B., Chen, C., Kwak, E.-S., Stein, B., Kao, C.C., 2003. J. Am. Chem. Soc. 125(21),
567 6374–6375.
568 Dutta Chowdhury, A., Ganganboina, A.B., Nasrin, F., Takemura, K., Doong, R.-a., Utomo,
569 D.I.S., Lee, J., Khoris, I.M., Park, E.Y., 2018. Anal. chem. 90(21), 12464–12474.
570 Ganganboina, A.B., Chowdhury, A.D., Khoris, I.M., Doong, R.-a., Li, T.-C., Hara, T., Abe, F.,
571 Suzuki, T., Park, E.Y., 2020a. Biosens. Bioelectron. 170, 112680.
572 Ganganboina, A.B., Chowdhury, A.D., Khoris, I.M., Nasrin, F., Takemura, K., Hara, T., Abe,
573 F., Suzuki, T., Park, E.Y., 2020b. Biosens. Bioelectron. 157, 112169.
574 Ganganboina, A.B., Doong, R.-a., 2018. Sens. Actuators, B 273, 1179–1186.
575 Ganganboina, A.B., Doong, R.-A., 2019. Sci. Rep. 9(1), 7214.
576 Ganganboina, A.B., Dutta Chowdhury, A., Doong, R.-a., 2018. ACS Appl. Mater. Interfaces
577 10(1), 614–624.
578 Ganganboina, A.B., Khoris, I.M., Chowdhury, A.D., Li, T.-C., Park, E.Y., 2020c. ACS Appl.
579 Mater. Interfaces 12 (45), 50212–50221.
580 Herbert, F.C., Brohlin, O.R., Galbraith, T., Benjamin, C., Reyes, C.A., Luzuriaga, M.A.,
581 Shahrivarkevishahi, A., Gassensmith, J.J., 2020. Bioconjugate Chem. 31(5), 1529–1536.
582 Iverson, G.M., Matsuura, E., Victoria, E.J., Cockerill, K.A., Linnik, M.D., 2002. J. Autoimmun
583 18(4), 289–297.
584 Lei, Y.-M., Zhou, J., Chai, Y.-Q., Zhuo, Y., Yuan, R., 2018. Anal. chem. 90(20), 12270–12277.
585 Li, L., Xu, C., Zhang, W., Secundo, F., Li, C., Zhang, Z.-P., Zhang, X.-E., Li, F., 2019a. Nano
586 lett. 19(4), 2700–2706.
587 Li, T.-C., Yamakawa, Y., Suzuki, K., Tatsumi, M., Razak, M., Uchida, T., Takeda, N.,
588 Miyamura, T., 1997. Journal of virology 71(10), 7207–7213.
589 Li, T.-C., Yoshimatsu, K., Yasuda, S.P., Arikawa, J., Koma, T., Kataoka, M., Ami, Y., Suzaki,
590 Y., Mai, L.T.Q., Hoa, N.T., 2011. J. Gen. Virol. 92(Pt 12), 2830.

Li, T.C., Bai, H., Yoshizaki, S., Ami, Y., Suzaki, Y., Doan, Y.H., Takahashi, K., Mishiro, S., Takeda, N., Wakita, T., 2019b. Hepatology communications 3(1), 160–172.

Liu, Y., Nie, Y., Wang, M., Zhang, Q., Ma, Q., 2020. Biosens. Bioelectron. 148, 111823.

Liu, Z., Qiao, J., Niu, Z., Wang, Q., 2012. Chem. Soc. Rev. 41(18), 6178–6194.

Ma, Y., Nolte, R.J., Cornelissen, J.J., 2012. Adv. Drug Delivery Rev. 64(9), 811–825.

Michalet, X., Pinaud, F.F., Bentolila, L.A., Tsay, J.M., Doose, S., Li, J.J., Sundaresan, G., Wu, A., Gambhir, S., Weiss, S., 2005. Science 307(5709), 538–544.

World Health Organization, W.H., 2015. Weekly Epidemiological Record Relevé épidémiologique hebdomadaire 90(18), 185–200.

Qi, H., Zhang, C., 2020. Anal. Chem. 2020, 92, 1, 524–534

Robinson, D.A., Stevenson, K.J., 2013. J. Mater. Chem. A 1(43), 13443–13453.

Sasaki, E., Dragoman, R.M., Mantri, S., Dirin, D.N., Kovalenko, M.V., Hilvert, D., 2020. ChemBioChem 21(1-2), 74–79.

Shrestha, A.C., Flower, R.L., Seed, C.R., Stramer, S.L., Faddy, H.M., 2016. *J. Blood Transfus.* 47(2), 97–100.

Tagit, O., De Ruiter, M., Brasch, M., Ma, Y., Cornelissen, J., 2017. RSC Adv. 7(60), 38110–38118.

Takahashi, M., Kusakai, S., Mizuo, H., Suzuki, K., Fujimura, K., Masuko, K., Sugai, Y., Aikawa, T., Nishizawa, T., Okamoto, H., 2005. J. Clin. Microbiol. 43(1), 49–56.

Takamura, S., Niikura, M., Li, T., Takeda, N., Kusagawa, S., Takebe, Y., Miyamura, T., Yasutomi, Y., 2004. Gene Ther. 11(7), 628–635.

Tsai, C.-t., Robinson, P.V., Spencer, C.A., Bertozzi, C.R., 2016. ACS Cent. Sci. 2(3), 139–147.

Wen, A.M., Steinmetz, N.F., 2016. Chem. Soc. Rev. 45(15), 4074–4126.

Wenzel, J.J., Preiss, J., Schemmerer, M., Huber, B., Jilg, W., 2013. J. Infect. Dis. 207(3), 497–500.

Yan, D., Wang, B., Sun, S., Feng, X., Jin, Y., Yao, X., Cao, S., Guo, H., 2015. PloS one 10(9), e0138883.

Yang, D., Qiu, Z., Cui, W., Shen, Z., Liu, W., Hu, H., Jin, M., Li, J.-W., 2017. Nanotechnol. Lett. 9(12), 2119–2125.

Yang, Y.-B., Tang, Y.-D., Hu, Y., Yu, F., Xiong, J.-Y., Sun, M.-X., Lyu, C., Peng, J.-M., Tian, Z.-J., Cai, X.-H., 2020. Nano Lett. 20(2), 1417–1427.

Zafrullah, M., Zhang, X., Tran, C., Nguyen, M., Kamili, S., Purdy, M.A., Stramer, S.L., 2018. Transfusion 58(5), 1254–1263.

Zhang, B., Kumar, R.B., Dai, H., Feldman, B.J., 2014. Nat. Med. 20(8), 948–953.

Supplementary data

Cargo encapsulated Hepatitis E virus-like particles for anti-HEV antibody detection

Akhilesh Babu Ganganboina[1], Kenshin Takemura[2], Wenjing Zhang[3], Tian-Cheng Li[3], Enoch Y. Park[1,2,*]

[1] Research Institute of Green Science and Technology, Shizuoka University, 836 Ohya Suruga-ku, Shizuoka 422-8529, Japan
[2] Department of Bioscience, Graduate School of Science and Technology, Shizuoka University, 836 Ohya Suruga-ku, Shizuoka 422-8529, Japan
[3] Department of Virology 2, National Institute of Infectious Diseases, 4-7-1 Gakuen, Musashimurayam-shi, Tokyo 208-0011, Japan

E-mail addresses:
akhilesh.babu.ganganboina@shizuoka.ac.jp (ABG)
takemura.kenshin.16@shizuoka.ac.jp (KT)
zwjviolin@foxmail.com (WZ)
litc@nih.go.jp (TCL)
park.enoch@shizuoka.ac.jp (EYP)

[*] Corresponding author at: Research Institute of Green Science and Technology, Shizuoka University, 836 Ohya, Suruga-ku, Shizuoka 422-8529, Japan.
E-mail address: park.enoch@shizuoka.ac.jp (E.Y. Park). Tel (Fax): +81-54-238-4887)

Table S1: Comparison of the other test platforms for antibody detection

No	Methodology	Nanomaterial	Linea range	LOD	Ref
1	Chemiluminescence	TiO_2	0.5 – 200 ng mL^{-1}	0.1 ng mL^{-1}	(Wang et al., 2012)
2		AuNPs	6×10^{-10} – 5.3×10^{-7} g mL^{-1}	3.2×10^{-11} g mL^{-1}	(Qi et al., 2014)
3		AuNPs	0.1 – 10.0 ng mL^{-1}	0.03 ng mL^{-1}	(Li et al., 2016)
4	Fluorescence	QD NBs	0.005 – 40 ng mL^{-1}	4 pg mL^{-1}	(Guo et al., 2020)
5		CuNCs	0.05 − 12 ng mL^{-1}	7 pg mL^{-1}	(Li et al., 2019)
6		CdSe QDs - SiO_2	N/A	0.05 ng mL^{-1}	(Wu et al., 2015)
7		Carbon dots	40 − 4000 ng mL^{-1}	150 pg mL^{-1}	(Song et al., 2018)
8		QD@HEV-LPs	10^{-13} – 10^{-7} g mL^{-1}	0.87 pg mL^{-1}	**(This work)**

QD NBs: quantum dot nanobeads, CuNCs: copper nanoclusters

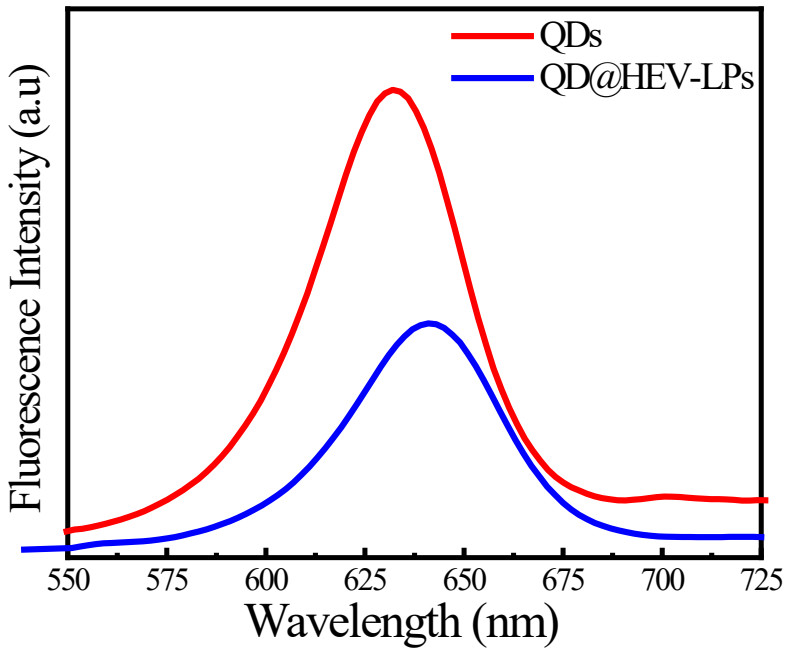

Fig. S1. Fluorescent emission spectra of QDs and QDs@HEV-LP

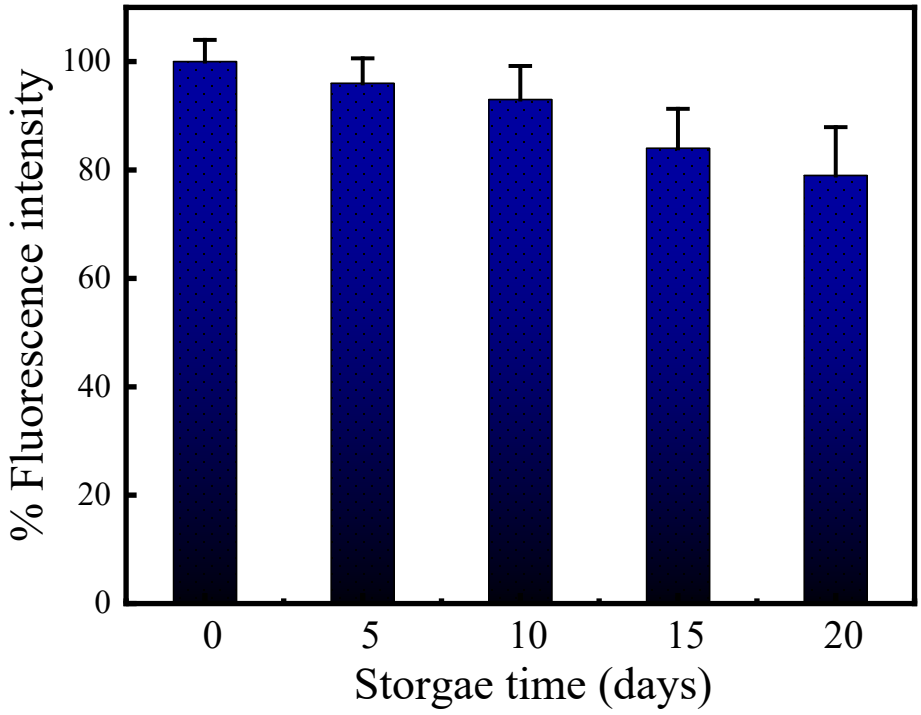

Fig. S2. Fluorescence intensity of QD@HEV-LPs during long term storage. Error bars denote data as average ± SD (n = 3).

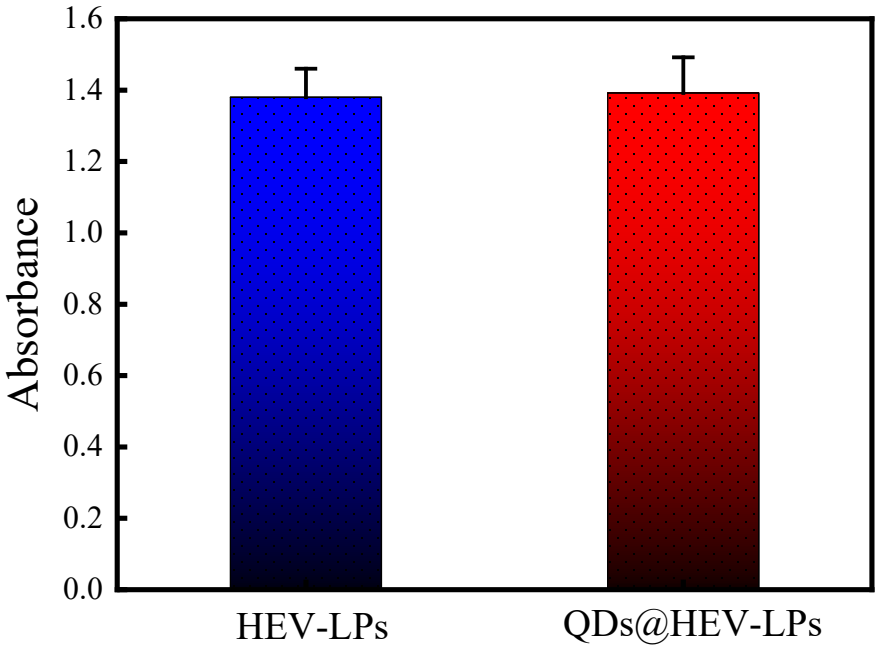

Fig. S3. Confirmation of antibody conjugation affinity by ELISA using 100 pg mL^{-1} of anti-HEV antibody for HEV-LPs and QD@HEV-LPs. The absorbance was measured at 450 nm. Error bars denote data as average ± SD (n = 3).

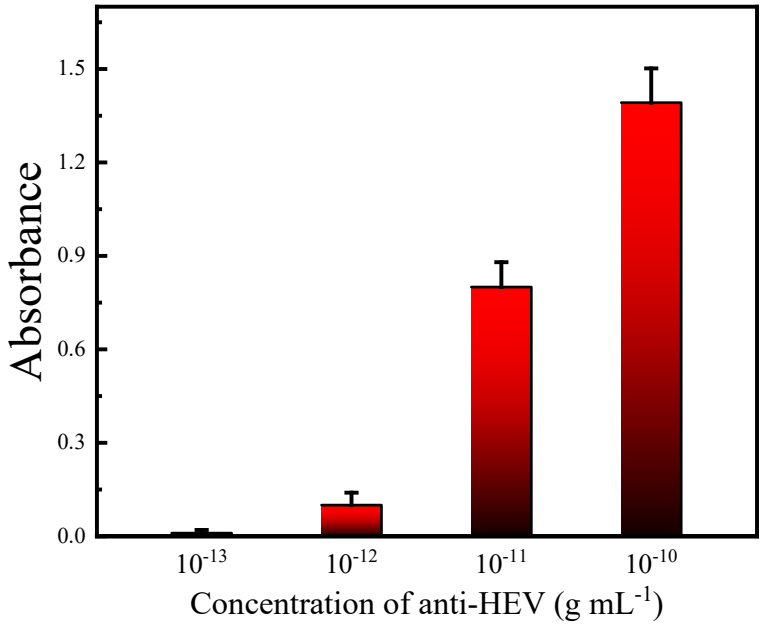

Fig. S4: ELISA for detecting anti-HEV antibody using QD@HEV-LPs and HRP conjugated anti-R-IgG antibodies. Error bars denote data as average ± SD (n = 3).

References

Guo, J., Wang, Y., Niu, S., Li, H., Tian, Y., Yu, S., Yu, F., Wu, Y., Liu, L.-e., 2020. ACS omega 5(36), 23229–23236.

Li, H., Zhao, M., Liu, W., Chu, W., Guo, Y., 2016. Talanta 147, 430–436.

Li, R., Liu, Q., Jin, Y., Li, B., 2019. Sens. Actuators, B 281, 28–33.

Qi, Y., Xiu, F.-R., Li, B., 2014. Anal. Biochem. 449, 1–8.

Song, P., Liu, Q., Zhang, Y., Liu, W., Meng, M., Yin, Y., Xi, R., 2018. RSC Adv. 8(1), 162–169.

Wang, Z., Han, J., Gao, H., Li, C., Fu, Z., 2012. Talanta 88, 765–768.

Wu, L., Li, X., Shao, K., Ye, S., Liu, C., Zhang, C., Han, H., 2015. Anal. Chim. Acta 887, 192–200.